

Topological-Fermi-Liquid to Quantum-Hall-Liquid Transitions: p -Band and d -Band Fermions in a Magnetic Field

Yi-Fei Wang¹ and Chang-De Gong^{1,2}

¹Center for Statistical and Theoretical Condensed Matter Physics,
and Department of Physics, Zhejiang Normal University, Jinhua 321004, China

²National Laboratory of Solid State Microstructures and Department of Physics, Nanjing University, Nanjing 210093, China
(Dated: March 30, 2022)

We find that in a multi-orbital system with intraorbital and interorbital hopping integrals, the Hall conductance exhibits various topological quantum phase transitions (QPTs) induced by on-site orbital polarization: integer quantum Hall (IQH) plateau transitions, and topological Fermi liquid to IQH transitions. Such topological QPTs are demonstrated in two systems: a p -band spinless fermionic system realizable with ultracold atoms in optical lattice, and a d -band spinful fermionic system closely related to giant orbital Hall effects in transition metals and their compounds.

PACS numbers: 73.43.Nq, 73.43.Cd, 03.75.Ss, 72.80.Ga

Introduction.— Orbital is an additional degree of freedom independent of charge and spin, and is characterized by orbital degeneracy and spatial anisotropy. Recently, it is proposed that novel p -orbital physics exist in optical lattices, and earlier attention has been paid on bosons in the first excited p -orbital bands [1]. Rapid experimental advances in loading and controlling alkali atoms on the excited bands makes the p -orbital physics truly fascinating [2, 3, 4], and especially a metastable p -orbital bosonic system has been realized [3]. Correlated fermions in the p -orbital bands possess more arresting behaviors, including Wigner crystallization, orbital ordering and frustration [5, 6, 7]. Even for non-interacting p -band spinless fermions, non-trivial topological band structures arises from lifting the orbital degeneracy, and Haldane’s quantum Hall model without Landau levels [8] can be realized [9].

In parallel, for transition metal oxides, the relevant active orbitals are the partially filled five d -orbitals. Recently, giant spin Hall and orbital Hall effects have been found in transition metals and their compounds [10, 11, 12], and many theoretical studies are based on realistic multiband $4d$ or $5d$ models [13, 14, 15]. A possible intrinsic origin of these giant Hall effects is the “orbital Aharonov-Bohm phase” which is induced by the on-site spin-orbital coupling (SOC) and the phase of interorbital hopping integrals characteristic of d -orbital systems, and therefore the conduction electrons are subject to an effective spin-dependent magnetic field [13, 14].

Given the intensive current interest in possible novel p -orbital and d -orbital physics which has not appeared in single-orbital systems, we are motivated to study magneto-transport properties of multi-orbital systems with intraorbital and interorbital hopping integrals modulated by an external magnetic flux, and find that the Hall conductance (HC) may exhibit various topological quantum phase transitions (QPTs) induced by on-site orbital polarization: integer quantum Hall (IQH) plateau transitions, and topological Fermi liquid (TFL) to IQH

transitions. An IQH effect, characterized by a nonzero Chern integer [16], only occurs when the Fermi level lies in an energy gap, and is a Fermi sea property. While the non-quantized part of the HC of a TFL is characterized by a Berry phase accumulated by adiabatic motion of quasiparticles on the Fermi surface (FS), and is thus purely a Fermi liquid property [17]. Such topological QPTs are demonstrated in two systems: a p -band spinless fermionic system which is proposed to be realized with ultracold atoms in optical lattice [9], and a d -band spinful fermionic system which is closely related to giant orbital Hall effect in transition metals and their compounds [13, 14].

Formulation.—The first model is a p -band system of p_x and p_y orbitals in a 2D square lattice filled with spinless fermions coupled with an artificial uniform magnetic flux [5, 6, 7, 9, 18]:

$$H_p = \sum_{\mathbf{r}} \sum_{\mu, \nu=x, y} [t_{\parallel} \delta_{\mu\nu} - t_{\perp} (1 - \delta_{\mu\nu})] \times [p_{\mu, \mathbf{r}}^{\dagger} p_{\mu, \mathbf{r} + \mathbf{e}_{\nu}} \exp(i\phi_{\mathbf{r}, \mathbf{r} + \mathbf{e}_{\nu}}) + \text{H.c.}] + \lambda \sum_{\mathbf{r}} (ip_{x, \mathbf{r}}^{\dagger} p_{y, \mathbf{r}} - ip_{y, \mathbf{r}}^{\dagger} p_{x, \mathbf{r}}), \quad (1)$$

where $p_{\mu, \mathbf{r}}^{\dagger}$ is a fermion creation operator of $\mu = x, y$ p -orbital at site \mathbf{r} . t_{\parallel} and t_{\perp} are the nearest neighbor (NN) hopping integrals in the longitudinal and transverse directions, respectively, to each p -orbital orientation. $t_{\parallel}, t_{\perp} > 0$, and t_{\perp} is conventionally one order of magnitude smaller than t_{\parallel} . In the following, t_{\parallel} will be taken as the unit of energy. A finite λ induces the rotation of each site around its own center, thus gives rise to orbital polarization by lifting the degeneracy between $p_x \pm ip_y$ orbitals [9, 18].

The second model is a d -band system of $d_{xz, \sigma}$ and $d_{yz, \sigma}$ orbitals (the notation is simplified as $d_{xz, \sigma} \equiv d_{x\sigma}$ and $d_{yz, \sigma} \equiv d_{y\sigma}$) in a 2D square lattice filled with spinful

fermions coupled with a uniform magnetic flux [13, 14]:

$$\begin{aligned}
H_d = & -t_{\parallel} \sum_{\mathbf{r}, \sigma, \mu} [d_{\mu\sigma, \mathbf{r}}^{\dagger} d_{\mu\sigma, \mathbf{r}+\mathbf{e}_{\mu}} \exp(i\phi_{\mathbf{r}, \mathbf{r}+\mathbf{e}_{\mu}}) + \text{H.c.}] \\
& + t' \sum_{\mathbf{r}, \sigma} [d_{x\sigma, \mathbf{r}}^{\dagger} d_{y\sigma, \mathbf{r} \pm \mathbf{e}_x \pm \mathbf{e}_y} \exp(i\phi_{\mathbf{r}, \mathbf{r} \pm \mathbf{e}_x \pm \mathbf{e}_y}) + \text{H.c.}] \\
& - t' \sum_{\mathbf{r}, \sigma} [d_{x\sigma, \mathbf{r}}^{\dagger} d_{y\sigma, \mathbf{r} \pm \mathbf{e}_x \mp \mathbf{e}_y} \exp(i\phi_{\mathbf{r}, \mathbf{r} \pm \mathbf{e}_x \mp \mathbf{e}_y}) + \text{H.c.}] \\
& + \lambda \sum_{\mathbf{r}} (id_{x\downarrow, \mathbf{r}}^{\dagger} d_{y\downarrow, \mathbf{r}} - id_{x\uparrow, \mathbf{r}}^{\dagger} d_{y\uparrow, \mathbf{r}} + \text{H.c.}), \quad (2)
\end{aligned}$$

where $d_{\mu\sigma, \mathbf{r}}^{\dagger}$ creates a fermion of $\mu = xz, yz$ d -orbital and spin $\sigma = \uparrow, \downarrow$ at site \mathbf{r} . t_{\parallel} is the NN intraorbital hopping integral in the longitudinal direction, and $\pm t'$ is the next NN interorbital hopping integrals. $t_{\parallel}, t' > 0$, and t' is one order of magnitude smaller than t_{\parallel} . And t_{\parallel} will also be taken as the energy unit. Here λ is the atomic SOC strength [13, 14], and it also causes orbital polarization, but with a spin dependence.

We consider $1/N$ magnetic flux quantum per plaquette (N is an integer), i.e. $\phi = \sum_{\square} \phi_{ij} = 2\pi Ba^2/\phi_0 = 2\pi/N$, with a the lattice constant and $\phi_0 = hc/e$ the flux quantum. The Landau gauge $\mathbf{A} = (0, -Bx, 0)$ and the periodical boundary conditions (PBCs) are adopted, and the magnetic unit cell has the size $N \times 1$. After the numerical diagonalization of the Hamiltonian, the zero-temperature HC is calculated through the Kubo formula [16]

$$\begin{aligned}
\sigma_{\text{H}}(E) = & \frac{ie^2\hbar}{A} \sum_{\mathcal{E}_{n\mathbf{k}} < E} \sum_{\mathcal{E}_{m\mathbf{k}} > E} \\
& \frac{\langle n\mathbf{k}|v_x|m\mathbf{k}\rangle \langle m\mathbf{k}|v_y|n\mathbf{k}\rangle - \langle n\mathbf{k}|v_y|m\mathbf{k}\rangle \langle m\mathbf{k}|v_x|n\mathbf{k}\rangle}{(\mathcal{E}_{m\mathbf{k}} - \mathcal{E}_{n\mathbf{k}})^2} \quad (3)
\end{aligned}$$

where $A = L \times L$ is the area of this 2D system, E is the Fermi energy, $\mathcal{E}_{n\mathbf{k}}$ is the corresponding eigenvalue of the eigenstate $|n\mathbf{k}\rangle$ of n th Landau subband, and the summation over wave vector \mathbf{k} is restricted to the magnetic Brillouin zone (MBZ): $-\pi/N \leq k_x a < \pi/N$ and $-\pi \leq k_y a < \pi$. The velocity operator is defined as $\mathbf{v} = (i/\hbar)[H, \mathbf{R}]$, with \mathbf{R} as the position operator of fermions. When E falling in energy gaps, we can rewrite σ_{H} as $\sigma_{\text{H}}(E) = \sum_{\mathcal{E}_n < E} \sigma_{\text{H}}^{(n)} = e^2/h \sum_{\mathcal{E}_n < E} C_n$, where $\sigma_{\text{H}}^{(n)}$ and C_n are the HC and the Chern number [16] of the n th completely filled subband, respectively.

Now let us introduce the Berry connection $\mathbf{A}_n(\mathbf{k}) = i\langle n\mathbf{k}|\nabla_{\mathbf{k}}|n\mathbf{k}\rangle$, and the Berry curvature $\Omega_n^z(\mathbf{k}) = \nabla_{\mathbf{k}} \times \mathbf{A}_n(\mathbf{k})$. With these definitions, the quantized HC of a completely filled n th subband can be written as $(h/e^2)\sigma_{\text{H}}^{(n)} = (1/2\pi) \int_{\text{MBZ}} \Omega_n^z(\mathbf{k}) d^2\mathbf{k} = (1/2\pi) \oint_{\text{MBZ}} \mathbf{A}_n(\mathbf{k}) \cdot d\mathbf{k} = \Gamma_{\text{MBZ}}^{(n)}/2\pi$, where $\Gamma_{\text{MBZ}}^{(n)}$ is the Berry phase of the cyclic evolution of the n th eigenstate $|n\mathbf{k}\rangle$ along the MBZ boundary [16]. While for a partially filled n th subband, the non-quantized part of the HC can also be written as $(h/e^2)\sigma_{\text{H}}^{(n)} = (1/2\pi) \oint_{\text{FS}} \mathbf{A}_n(\mathbf{k}) \cdot d\mathbf{k} =$

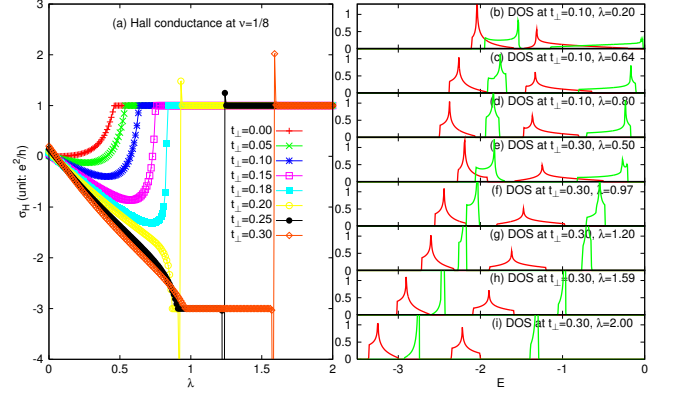


FIG. 1: (color online). (a) Hall conductivity versus λ (unit: t_{\parallel}) of p -band spinless fermions at $\nu = 1/8$ with $N = 4$ and various t_{\perp} 's. (b)-(i) The DOS for some t_{\perp} 's and λ 's in (a).

$\Gamma_{\text{FS}}^{(n)}/2\pi$, where $\Gamma_{\text{FS}}^{(n)}$ now is the Berry phase of the cyclic evolution of $|n\mathbf{k}\rangle$ along the FS [17]. It is also instructive to introduce the sum of Berry curvatures over the occupied subbands (for each \mathbf{k}): $\Omega^z(\mathbf{k}) = \sum_{\mathcal{E}_n < E} \Omega_n^z(\mathbf{k})$.

p-band spinless fermions. (a) Hall conductances.—An overall picture of the HC σ_{H} calculated by Eq. (3) is shown in Fig. 1 for p -band spinless fermions [Eq. (1)] with $N = 4$ (i.e., the flux strength $\phi = \frac{1}{4} \times 2\pi$), 2048×2048 lattice sites, fermion filling $\nu = 1/8$, and various t_{\perp} 's.

In the case of $\lambda = 0$, the lowest two subbands (each contributes $\frac{1}{8}$ to ν) are not separated; they give rise to a total Chern number $+2$. With λ increasing from 0 to 2.0 one sees a systematic evolution of σ_{H} versus λ ; for smaller t_{\perp} 's, there is a quantum critical point (QCP) λ_{c1} at which the lowest two subbands begin to separate; for larger t_{\perp} 's, besides the first QCP λ_{c1} , there is another QCP λ_{c2} at which σ_{H} exhibit a quantized jump.

At smaller t_{\perp} 's ($t_{\perp} = 0.00, \dots, 0.18$), for $\lambda > \lambda_{c1}$ (e.g. $\lambda_{c1} \simeq 0.64$ for $t_{\perp} = 0.10$), the lowest two subbands are well separated since λ lifts the p -orbital degeneracy and induces a finite energy gap; the lowest subband is occupied by $p_x + ip_y$ fermions while the second lowest one by $p_x - ip_y$ fermions, each subband carrying a Chern number $+1$, and $\sigma_{\text{H}} = +1e^2/h$ (i.e. $C_1 = +1$) at $\nu = 1/8$.

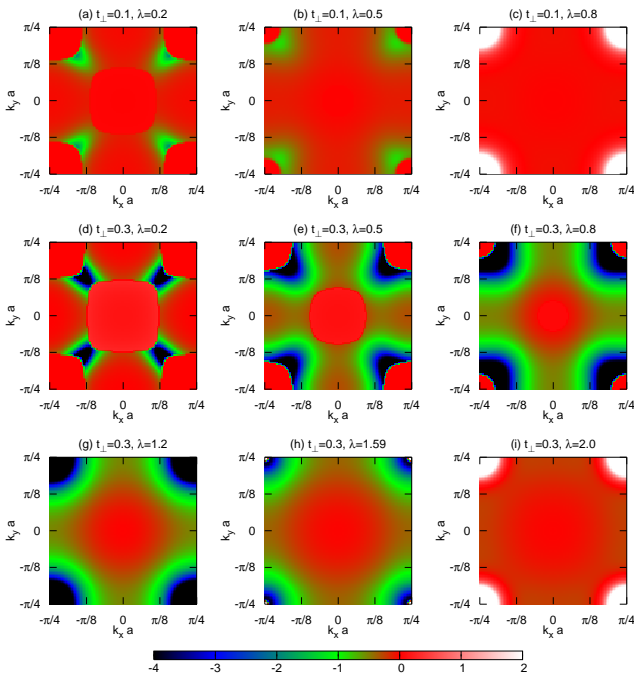
At larger t_{\perp} 's ($t_{\perp} = 0.20, 0.25, 0.30$), for $\lambda > \lambda_{c1}$ (e.g. $\lambda_{c1} \simeq 0.97$ for $t_{\perp} = 0.30$), the lowest two subbands are also well separated; however, the lowest subband occupied by $p_x + ip_y$ fermions now gives a Chern number $C_1 = -3$. When λ increases further to another QCP λ_{c2} (e.g. $\lambda_{c2} \simeq 1.59$ for $t_{\perp} = 0.30$), σ_{H} exhibit a quantized jump from $-3e^2/h$ to $+1e^2/h$ at $\nu = 1/8$ (i.e. C_1 changes from -3 to $+1$).

The above behaviors of HCs have also been verified by further numerical calculations of the cases with $N = 6 - 16$, various t_{\perp} 's, and various ν 's (Table I).

(b) Berry curvatures.—In order to reveal the non-trivial topological properties, we plot in Fig. 2 the Berry curvatures $\Omega^z(\mathbf{k})$, in the reduced MBZ (RMBZ)

TABLE I: Topological QPTs of p -band spinless fermions.

(N, ν, t_{\perp})	λ_{c1}	λ_{c2}	quantized jump of σ_H at λ_{c2}
(6, 1/12, 0.25)	0.70	1.16	$-5e^2/h \rightarrow +1e^2/h$
(8, 1/16, 0.20)	0.50	0.89	$-7e^2/h \rightarrow +1e^2/h$
(8, 3/16, 0.25)	0.41	0.59	$-5e^2/h \rightarrow +3e^2/h$
(12, 1/24, 0.20)	0.42	0.92	$-11e^2/h \rightarrow +1e^2/h$
(12, 3/24, 0.20)	0.29	0.45	$-9e^2/h \rightarrow +3e^2/h$
(16, 1/32, 0.10)	0.24	0.44	$-15e^2/h \rightarrow +1e^2/h$
(16, 3/32, 0.20)	0.26	0.53	$-13e^2/h \rightarrow +3e^2/h$
(16, 5/32, 0.20)	0.20	0.26	$-11e^2/h \rightarrow +5e^2/h$

FIG. 2: (color online). Intensity plots of Berry curvatures $\Omega^z(\mathbf{k})$ in the RMBZ of p -band fermions at $\nu = 1/8$ with $N = 4$, various t_{\perp} 's and λ 's.

$(-\pi/N \leq k_x a, k_y a < \pi/N)$ for some typical parameters corresponding to Fig. 1.

We first look into the case of $t_{\perp} = 0.1$ which has only one λ_c (see Fig. 1). For $\lambda < \lambda_{c1} \simeq 0.64$, e.g. $\lambda = 0.2$ [Fig. 2(a)], $\Omega^z(\mathbf{k})$ displays the FS topology of two subbands: a hole FS of the lowest subband near four corners of the RMBZ, and a fermion FS of the second lowest subband near the center of the RMBZ. There are four small negative- $\Omega^z(\mathbf{k})$ regions near the hole FS. When λ increases, the two subbands starts to separate and two FSs shrinks gradually [Fig. 2(b)]. For $\lambda > \lambda_{c1}$, e.g. $\lambda = 0.8$ [Fig. 2(c)], the two subbands separates completely, both FSs vanishes, and $\Omega^z(\mathbf{k})$ displays four maxima at the four RMBZ corners (these maxima contribute to the quantized $C_1 = +1$).

We then analyze the case of $t_{\perp} = 0.3$ which has two

λ_c 's (see Fig. 1). For a small $\lambda = 0.2$ [Fig. 2(d)], $\Omega^z(\mathbf{k})$ also displays the FS topology of two subbands. $\Omega^z(\mathbf{k})$ displays four negative regions between the hole and particle FSs. When λ increases, e.g. $\lambda = 0.5, 0.8$ [Figs. 2(e) and (f)], negative- $\Omega^z(\mathbf{k})$ regions also increase, change their topology, and enclose the four RMBZ corners, with the two FSs shrinking. When λ increases and passes $\lambda_{c1} = 0.97$, e.g. $\lambda = 1.2$ [Fig. 2(g)], the two subbands separates completely, and both FSs vanishes, and $\Omega^z(\mathbf{k})$ displays four negative- $\Omega^z(\mathbf{k})$ minima at the four RMBZ corners (these minima contribute to the quantized $C_1 = -3$). Near $\lambda_{c2} \simeq 1.59$ [Fig. 2(h)], four negative- $\Omega^z(\mathbf{k})$ minima at the RMBZ corners begin to vanish. When λ increases further and passes λ_{c2} , e.g. $\lambda = 2.0$ [Fig. 2(i)], the two subbands separates completely and four negative- $\Omega^z(\mathbf{k})$ minima vanishes, and are replaced by positive- $\Omega^z(\mathbf{k})$ maxima at the RMBZ corners (these maxima contribute to the quantized $C_1 = +1$ again).

(c) *Edge states.*—An alternative way to reveal different topological characters and QPTs is to calculate the edge states [19]. Now as an illustration, we take a cylinder of square lattice of the size $64 \times \infty$ with $N = 4$ (i.e., the flux strength $\phi = \frac{1}{4} \times 2\pi$), $t_{\perp} = 0.30$ and various λ 's, and apply open boundary condition (OBC) in x direction and PBC in y direction.

Chern numbers of the bulk subbands are intimately related to the winding numbers of the corresponding edge states [19]. We here concentrate on the edge states between the lowest two subbands shown in Fig. 3. For $0 < \lambda < \lambda_{c1} \simeq 0.97$ (see the $t_{\perp} = 0.30$ curve in Fig. 1), e.g. $\lambda = 0.50$ [Fig. 3(a)], there is one edge state winding between the lowest two subbands, however, the Chern number of the lowest subband C_1 is not well defined since the energy overlap of the two subbands. For $\lambda_{c1} < \lambda < \lambda_{c2} \simeq 1.59$, e.g. $\lambda = 1.20$ [Fig. 3(b)], there is one edge state winding three times from the lowest subband to the upper one then back to the lowest one which corresponds to $C_1 = -3$. While $\lambda > \lambda_{c2}$, e.g. $\lambda = 2.00$ [Fig. 3(d)], there is another edge state winding only once from the upper subband to the lowest one then back to the upper one which corresponds to $C_1 = +1$.

The continuum spectra of this cylinder also give further descriptions about the correspondence between the quantized jumps of the HCs and the topological evolutions of bulk spectra [8, 20, 21]. When approaching λ_{c2} , four pairs of Dirac cones begin to form between the lowest two subbands, and each pair of Dirac cones touch at one Dirac point when $\lambda_{c2} \simeq 1.59$ [Fig. 3(c)]. Meanwhile, a topological QPT happens at λ_{c2} , and a Chern number $+4$ is transferred from the upper subband to the lowest one, through abrupt changes of Berry curvatures near Dirac points [Fig. 2(h)]. On contrary, at the first QCP $\lambda_{c1} \simeq 0.97$, there is no Dirac point, and thus no quantized jumps of the HC.

d-band spinful fermions.—Some typical examples of the HC σ_H calculated by Eq. (3) are shown in Fig. 4

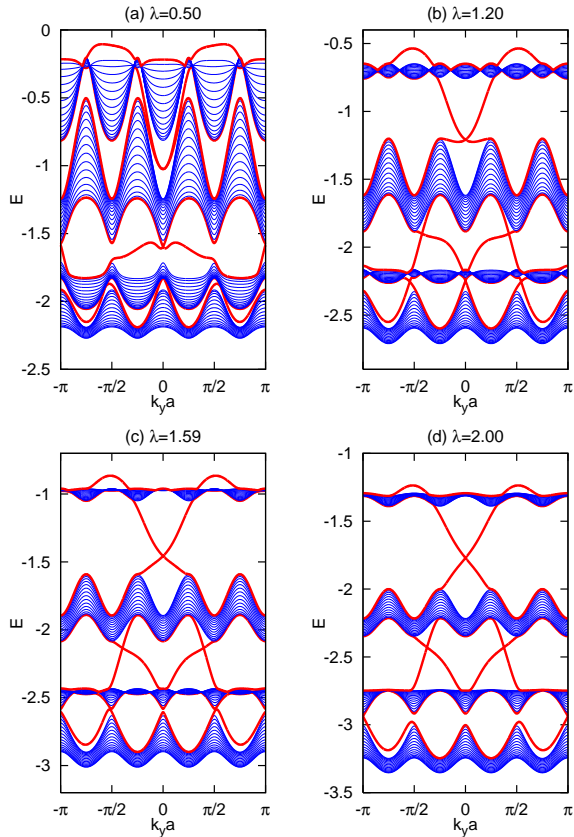


FIG. 3: (color online). $E(k_y)$ of lowest four subbands and edge states [shown as thick (red) lines] of p -band fermions in a $64 \times \infty$ cylinder with $t_{\perp} = 0.30$ and various λ 's.

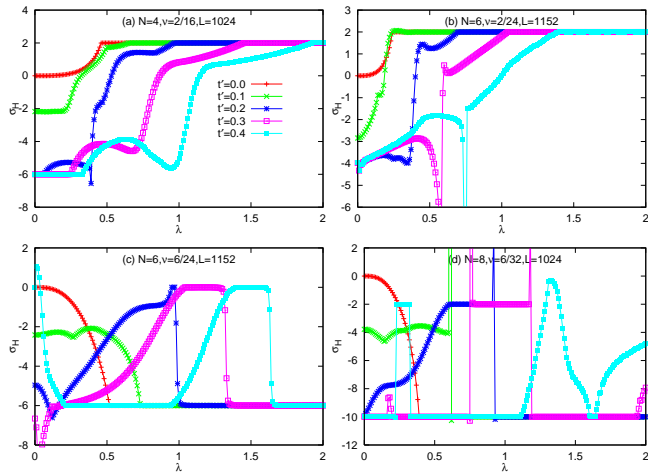


FIG. 4: (color online). σ_H (unit: e^2/h) versus λ (unit: t_{\parallel}) of d -band spinful fermions at various N 's, ν 's and t' 's.

for d -band spinful fermions [Eq. (2)] with various N 's, ν 's and t' 's. We note that TFL-to-IQH transitions occur frequently when tuning λ to critical values λ_c 's. Since now we have two spin components, σ_H may change either $2Ne^2/h$ [e.g. the $t' = 0.3$ case in Fig. 4(a)] or Ne^2/h [e.g. the $t' = 0.4$ case in Fig. 4(c)], after passing a TFL region

or a quantized jump.

Summary and discussion.—We present that in a multi-orbital system with intraorbital and interorbital hopping integrals, the HC may exhibit various topological QPTs induced by on-site orbital polarization: IQH plateau transitions, and TFL to IQH transitions. Berry curvatures and edge states give further insights to reveal different topological characters and QPTs. Such topological QPTs are demonstrated in both a p -band spinless fermionic system in optical lattice, and a d -band spinful fermionic system related to giant orbital Hall effects in transition metals and their compounds. In optical lattices, artificial magnetic fields can be created by laser assisted tunneling between internal atomic states, or time-varying quadrupole potential [22].

This work was supported by the National Natural Science Foundation of China (No. 10904130), the State Key Program for Basic Researches of China (No. 2006CB921802), and the Start-Up Funding at ZJNU.

-
- [1] A. Isacsson and S. M. Girvin, Phys. Rev. A **72**, 053604 (2005); W. V. Liu and C. Wu, *ibid.* **74**, 013607 (2006); A. B. Kuklov, Phys. Rev. Lett. **97**, 110405 (2006); C. Wu, W. V. Liu, J. E. Moore, and S. Das Sarma, *ibid.* **97**, 190406 (2006).
 - [2] M. Köhl *et al.*, Phys. Rev. Lett. **94**, 080403 (2005).
 - [3] T. Müller, S. Fölling, A. Widera, and I. Bloch, Phys. Rev. Lett. **99**, 200405 (2007).
 - [4] M. Anderlini *et al.*, Nature (London) **448**, 452 (2007).
 - [5] C. Wu, D. Bergman, L. Balents, and S. Das Sarma, Phys. Rev. Lett. **99**, 070401 (2007).
 - [6] C. Wu, Phys. Rev. Lett. **100**, 200406 (2008).
 - [7] E. Zhao and W. V. Liu, Phys. Rev. Lett. **100**, 160403 (2008).
 - [8] F. D. M. Haldane, Phys. Rev. Lett. **61**, 2015 (1988).
 - [9] C. Wu, Phys. Rev. Lett. **101**, 186807 (2008).
 - [10] S. O. Valenzuela and M. Tinkham, Nature (London) **442**, 176 (2006).
 - [11] N. P. Stern *et al.*, Phys. Rev. Lett. **97**, 126603 (2006).
 - [12] T. Kimura *et al.*, Phys. Rev. Lett. **98**, 156601 (2007).
 - [13] H. Kontani *et al.*, Phys. Rev. Lett. **100**, 096601 (2008); *ibid.* **102**, 016601 (2009).
 - [14] T. Tanaka *et al.*, Phys. Rev. B **77**, 165117 (2008); T. Tanaka and H. Kontani, *ibid.* **77**, 195129 (2008).
 - [15] G. Y. Guo, S. Murakami, T. W. Chen, and N. Nagaosa, Phys. Rev. Lett. **100**, 096401 (2008).
 - [16] D. J. Thouless, M. Kohmoto, M. P. Nightingale, and M. den Nijs, Phys. Rev. Lett. **49**, 405 (1982).
 - [17] F. D. M. Haldane, Phys. Rev. Lett. **93**, 206602 (2004).
 - [18] R. O. Umucalilar and M. Ö. Oktel, Phys. Rev. A **78**, 033602 (2008).
 - [19] Y. Hatsugai, Phys. Rev. Lett. **71**, 3697 (1993).
 - [20] Y. Hatsugai and M. Kohmoto, Phys. Rev. B **42**, 8282 (1990).
 - [21] Y. F. Wang and C. D. Gong, Phys. Rev. Lett. **98**, 096802 (2007); Y. F. Wang, Y. Zhao, and C. D. Gong, Phys. Rev. B **78**, 045301 (2008).
 - [22] D. Jaksch and P. Zoller, New J. Phys. **5**, 56 (2003); E.

J. Mueller, Phys. Rev. A **70**, 041603(R) (2004); A.S. Sørensen, E. Demler, and M. D. Lukin, Phys. Rev. Lett. **94**, 086803 (2005); K. Osterloh *et al.*, *ibid.* **95**, 010403

(2005); Y. J. Lin, *et al.*, *ibid.* **102**, 130401 (2009)